Design and Commissioning of an Ionization Intensity Monitor

A thesis presented for the degree of
Bachelor of Physics
Project duration: 2 months
Spring 2019

Hanna Berg
Supervised by Per Johnsson and Jasper Peschel

LUNDS UNIVERSITET

Division of Atomic Physics
Department of Physics

Design and Commissioning of an Ionization Intensity Monitor

Hanna Berg

Abstract

The dynamics of molecules and electrons takes place on timescales of femtoseconds and attoseconds, respectively. This requires ultrashort and intense extreme ultraviolet (XUV) pulses to be able to study them. Two sources that can generate intense XUV pulses are free-electron lasers (FELs) based on self amplified spontaneous emission (SASE) and high-order harmonic generation (HHG) driven by intense infrared (IR) laser.

At the Lund attosecond science centre (LASC) the intense XUV beamline generates XUV pulses via HHG. To accomplish ultrashort and intense XUV pulses it is essential to have methods for alignment and photon flux diagnostics.

In this work I have designed an ionization intensity monitor (IIM) and integrated it in the intense XUV beamline at LASC, with the purpose of measuring the photon flux of the generated XUV pulses. The design of the IIM is inspired by gas monitor detectors (GMDs) currently used at the soft X-ray FEL in Hamburg (FLASH) [1].

The working principle of the IIM is based on photoionization of rare gases and during commissioning it was shown that the IIM is sufficiently sensitive to XUV pulses to obtain both an ion and an electron signal. Performed single shot measurements determine the correlation between travel time of charge carriers and induced potential. By varying the energy of the generating IR pulses we investigate the linearity between the number of generated electrons and the photon flux of the XUV pulses.

Acronyms and Abbreviations

IIM	Ionization Intensity Monitor
GMD	Gas Monitor Detector
XUV	Extreme ultraviolet
IR	Infrared
VUV	Vacuum Ultraviolet
HHG	High-order Harmonic Generation
SASE	Self Amplified Spontaneous Emission
DB	Decoupling Box
LASC	Lund Attosecond Science Center
FEL	Free-Electron Laser
FLASH	Free-electron LASer in Hamburg
CPA	Chirped Pulse Amplification

Contents

Chapter 1

Introduction

Since the invention of the laser by Theodor Maiman in 1960 [2] laser pulses have become versatile tools to investigate matter. The shorter the object we want to observe, the smaller is the time scale that we need to access. The dynamics of molecules and electrons takes place on timescales of femtoseconds and attoseconds, respectively. This requires ultrashort and intense extreme ultraviolet (XUV) pulses in order to study them. Two sources that can generate intense XUV pulses are free-electron lasers (FELs) based on self amplified spontaneous emission (SASE) and high-order harmonic generation (HHG), driven by intense infrared (IR) pulses.
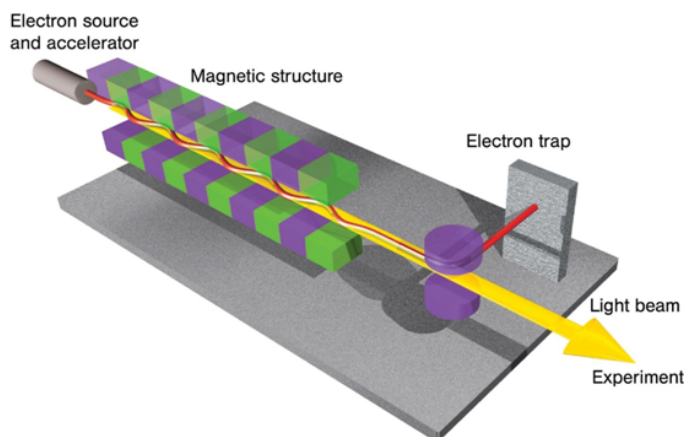

Figure 1.1: Schematic of a free-electron laser. Figure reproduced from reference [3].

In SASE-based FELs, bunches of electrons are generated by a pulsed source and linearly accelerated to relativistic velocities into a periodic structure of dipole magnets, called an undulator, see figure 1.1. When the electron bunches enter the undulator they will be accelerated in the perpendicular direction with respect to their velocity, and emit synchrotron radiation. The radiation is emitted in a cone in the same direction as the velocity of the electrons. The electrons interact with the emitted radiation at each undulator period and so-called periodic microbunches of electrons are created. The consequence is that the radiation is emitted with the same phase at every undulator period, and thus gets amplified [5]. This process provides laser pulses on the femtosecond timescale. Several facilities use this method to provide radiation in the XUV regime; one of them is

the free-electron laser in Hamburg (FLASH) [1], where the pulses can be used to investigate e.g. multiphoton excitation of atoms and molecules.
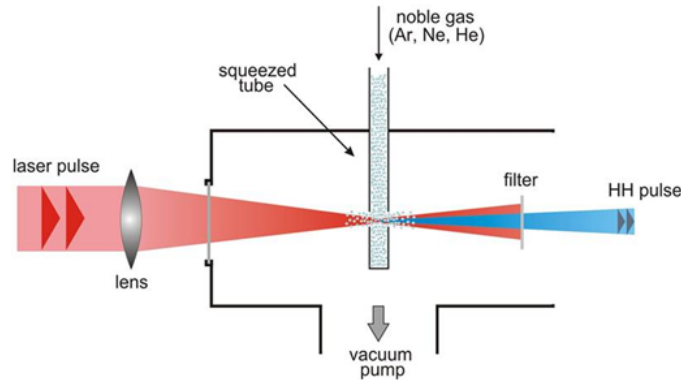

Figure 1.2: Schematic of an experimental set up of high-order harmonic generation driven by an IR laser. Figure reproduced from reference [4].

HHG is a non-linear process obtained when an intense laser pulse is focused into a target, see figure 1.2. When the target is a gas of atoms the atomic potential is distorted allowing tunnel ionization. The quasi-free electrons are accelerated in the electric field of the driving laser and might return to the remaining ion and recombine under the emission of XUV radiation [6]. The remaining radiation of the driving laser can be filtered away with optical devices. This process generates XUV pulses on the attosecond timescale, which can be used to investigate dynamics of electrons in atoms and molecules.

The peak power of highly energetic XUV pulses is much higher than their average power. If the radiation is focused into a spot of a few micrometer in diameter the peak intensity can reach above $10^{13} W/cm^2$ [7]. To be able to understand the non-linear processes and their intensity dependence it is important with diagnostics of several quantities, such as pulse energy, pulse duration and spot size of the intense XUV pulses. Researchers at FLASH have developed a detector for online measurement of the photon flux [1], which is an ionization intensity monitor (IIM) based on photoionization of rare gases.

At the Lund attosecond science centre (LASC) researchers want to investigate dynamics of electrons in atoms and molecules. This requires intense and ultrashort XUV pulses. In the intense XUV beamline at LASC, XUV pulses with pulse durations in the attosecond regime are obtained via HHG. The created XUV pulses are sufficiently intense to induce non-linear effects in matter [8].

In order to measure the photon flux of the XUV pulses, an XUV photodiode integrated after the experimental chamber, where the experiments are conducted, can be used. However, after generation of XUV pulses and before the experimental chamber a various number of XUV optics are integrated which affect the XUV pulses that are generated. This prevents the photodiode from measuring the photon flux online.

In this work an IIM, based on the device developed and used at FLASH [1], has been designed and integrated inside of the generation chamber, in the intense XUV beamline at LASC. The working principle of the IIM is based on the process of photoionization of rare gases with intense and pulsed XUV radiation. The IIM

consist of two electrodes, when an electric field is applied between the plates it collects charge carriers.

Commissioning of the IIM has shown that it is sufficiently sensitive to XUV pulses to obtain signal from both ions and electrons. A scan of the generating IR pulse energy indicates the linearity between the number of generated electrons and the photon flux of the XUV pulses. Through single-shot measurements, with different voltages applied to the IIM, the correlation between the travel time of the charge carriers and the applied potential was confirmed.

In this thesis chapter 2 gives an introduction to currently used IIMs at X-ray facilities, the working principle of the photoionization process and how to detect charge carriers are described and the chapter ends with a brief overview of the intense XUV beamline in Lund. The design and commissioning of an IIM is described in chapter 3, together with the procedures for the data analysis. In chapter 4 the results of the commissioning of the IIM is stated and discussed and chapter 5 gives a summary and outlook of the work done in this thesis.

Chapter 2

Background

In this chapter an introduction to IIMs used at current X-ray FEL facilities is given. The working principle of the photoionization process and how to detect charge carriers is described. In section 2.3 a brief overview of the intense XUV beamline in Lund is presented.

2.1 Ionization intensity monitors used at FEL facilities

Researchers have developed IIMs for online photon diagnostics at X-ray FEL facilities [1, 7, 9]. The pioneering work of the IIMs were performed at FLASH. Today they are used at all FEL facilities and are called gas monitor detectors (GMDs).

In figure 2.1 a schematic of a GMD currently used at FLASH is shown. The working principle of the GMDs at FLASH is based on photoionization of gases with a gas pressure in the range of 10^{-5} Pa (10^{-5} mbar). When radiation enters the GMD the target gas atoms are ionized. A homogeneous electric field accelerates the charge carriers towards electrodes where they are detected. The electronics provides single pulse read out for both electron and ion signal, which can be measured simultaneously.

Figure 2.1: A schematic of a GMD currently used at FLASH. Figure reproduced from reference [1].

With the GMD the absolute number of photons in each shot of highly intense and pulsed vacuum ultraviolet, (VUV) and XUV radiation can be determined with an accuracy of 10 percent [9]. The calibration of the GMDs was performed in the laboratory of the Physikalisch-Technische Bundeanstalt at the electron storage ring Bessy II in Berlin and the GMDs are currently used for online photon diagnostics at FLASH. For the calibration of the GMDs researchers used dispersed synchrotron radiation
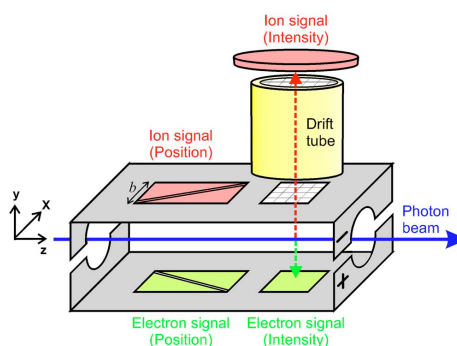
in the microwatt regime and a calibrated photodiode as the standard detector [1].

As observed in figure 2.1 the GMDs also allow determination of the position of the photon beam. We also see a drift tube in the ion path that allow time-of-flight measurements of ions, which makes differentiation between ion charge states possible. However, neither of these parts will be further discussed in this work.

2.2 Working principle

2.2.1 Photoionization

When a photon with sufficient energy interacts with an atom the atom might absorb the photon and eject an electron so that the atom becomes ionized. This process is called photoionization and an illustration is shown in figure 2.2. The energy of the incoming photon is denoted as $h\nu$, where h is Planck's constant, ν is the frequency of the photon and the electron ejected carries a kinetic energy E_{e^-}.

E_{e^-}

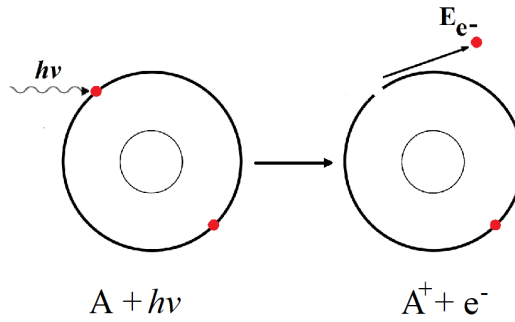$h\nu$

$A + h\nu$ $A^+ + e^-$

Figure 2.2: Schematic of the photoinonization process. The incident photon is absorbed by the atom and the atom ejects an electron.

For the electron to escape, the energy of the incoming photon needs to overcome the potential that binds the electron to the atom [10]. The kinetic energy of the electron is given by

$$\frac{1}{2}m_e v_e^2 = h\nu - I_p \tag{2.1}$$

where m_e is the mass of the electron, v_e is the velocity of the electron $h\nu$ is the energy of the photon and I_p is ionization potential. The minimum energy required for the photon to ionize the atom is called the threshold energy.

Imagine that we impinge a rare gas with pulsed radiation. The probability for a photon to ionize an atom depends on the photoionization cross sections of the target atom. For rare gases the photoionization cross-section, σ, is well known in the photon energy range of the threshold for respective rare gas and up to 125 eV [12]. From the generalized definition of the photoionization cross section [13] the number of generated ions/electrons per radiation pulse, $N_{ions/electrons}$, in the photoionization process is given by

$$N_{ions/electrons} = N_a \sigma_a F \tau. \tag{2.2}$$

where N_a is number of atoms in the target gas, σ_a is the photoionization cross section of the target, F the photon flux and τ is the pulse length. The flux of photons is a measure of number of photons, N_{ph}, per unit area, A and unit time τ, hence the expression to the right in equation 2.2 can be expressed as

$$\frac{N_a \sigma_a N_{ph} \tau}{A \tau} = n \sigma_a N_{ph} L \rightarrow N_{ions/electrons} = n \sigma_a N_{ph} L \qquad (2.3)$$

where n is the number density of the target gas and L is the length of the ionization path.

2.2.2 Ion and electron dynamics

Electrons and ions, generated in the photoionization process, are charge carriers and can be accelerated and directed by an electric field. The mobility of the charge carriers depends on its respective mass. By assuming that the initial velocity of the charge carriers is zero at time zero, Newtons second law, $\bar{F} = m d^2 \bar{x}/dt^2$, can be applied to derive an expression for the velocity of the charge carriers. Since the electric field, $\bar{E}$, is by definition the force per unit charge, $\bar{F}/q$, [14] we can express the velocity as a function of the electric field.

$$\bar{E} = \frac{\bar{F}}{q} = \frac{m}{q} \frac{d^2 \bar{x}}{dt^2} \rightarrow \frac{d\bar{x}}{dt} = \frac{\bar{E}q}{2m} t \qquad (2.4)$$

where m is the mass of the charge carrier, $d^2\bar{x}/dt^2$ is the acceleration, $d\bar{x}/dt$ is the velocity of the charger carrier and t is the time.
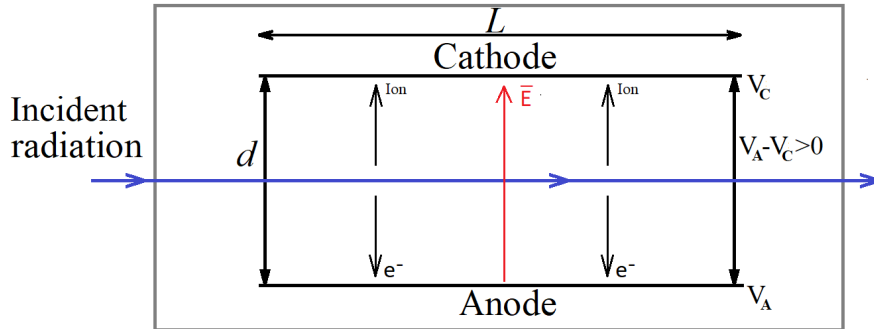
2.2.3 Detection and electronics

Figure 2.3: A schematic of an ionization chamber. Incident radiation ionizes gas atoms along its path, i.e the length, L, of the electrodes. The potential difference, $V_A - V_C$, generates an electric field, $\bar{E}$, between the electrodes. The electric field accelerates the electrons and the ions towards the anode and cathode, respectively.

A classical and widely used method of ionizing gas atoms is to use an ionization chamber [10, 11]. In figure 2.3 an illustration of an ionization chamber is shown. In this description we will consider the electrodes inside of the chamber to be

parallel with respect to each other. The chamber is filled with a target gas of well known density. When radiation enters the chamber the photons will ionize the gas atoms creating ions and electrons.

When an external voltage is applied to the electrodes the potential difference, $V_A - V_C$, generates an electric field between the electrodes. If the distance, d, between the electrodes is much smaller than the length, L, of the electrodes the electric field can be assumed to be homogeneous, indicated by red arrow in figure 2.3. The magnitude of the electric field created between the electrodes is defined as the potential between the plates divided by the distance between the plates, $E = (V_A - V_C)/d$ [15]. As described in the previous section, the electric field will accelerate the electrons and the ions against and along the direction of the electric field, respectively. This will generate a current of charges towards each electrode. From equation 2.4 and the definition, $E = (V_A - V_C)/d$, for the electric field we can derive a new expression for the velocity of a charge carrier as a function of the induced potential,

$$\frac{d\bar{x}}{dt} = \frac{(V_A - V_C)}{d}\frac{q}{m}t. \tag{2.5}$$

The ionization occurs at $x(t = 0) = 0$. The time it takes for the charge carriers to reach their respective electrode (at $x = d/2$) is given by

$$x = \frac{(V_A - V_C)}{d}\frac{q}{m}t^2 \iff t = d\sqrt{\frac{m}{q(V_A - V_C)}}. \tag{2.6}$$
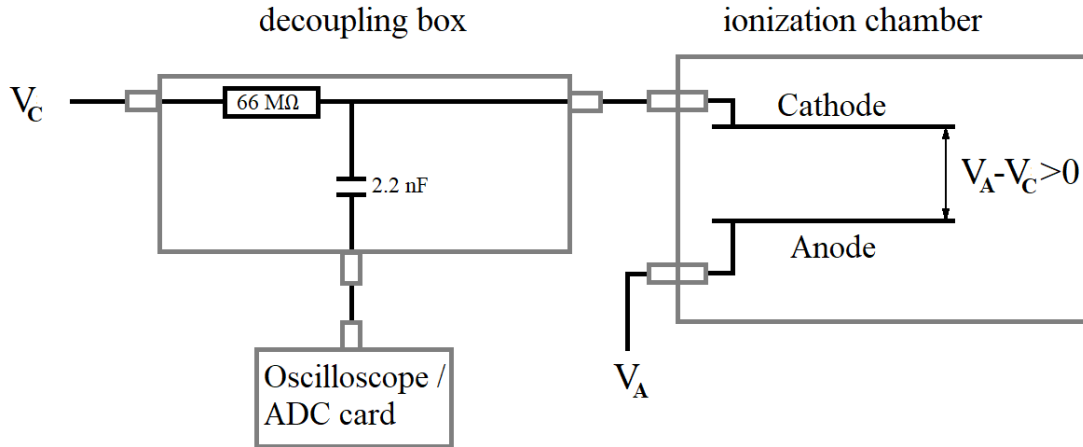

Figure 2.4: An illustration of an experimental setup for measurement of current generated due to photoionization.

In figure 2.4 a schematic of an experimental set up to measure the signal generated by the current is shown. The electrodes are connected to power supplies to generate an electric field between the electrodes. As radiation is sent through the ionization chamber this generates an electrical signal which is composed of a time dependent (AC) component and a constant (DC) component. This signal is put through the decoupling box (DB), which separates the two components

and directs the time dependent signal into the oscilloscope/ADC card where it is measured.
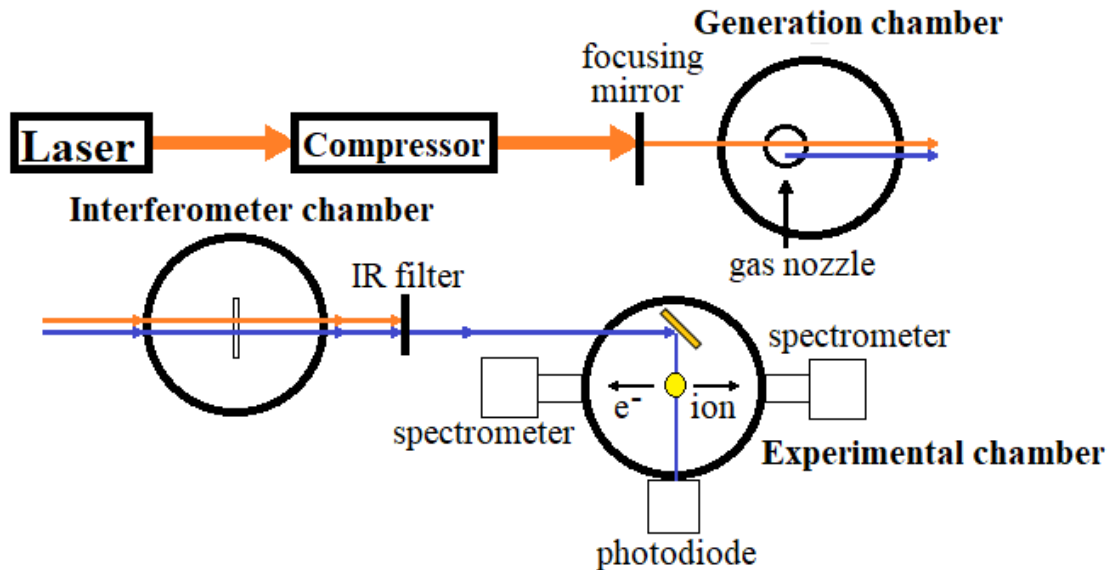
2.3 The intense XUV beamline in Lund

Figure 2.5: The XUV beamline. Red arrows indicate IR while blue arrows indicate XUV.

In this section a brief introduction of the intense XUV beamline in Lund is presented. An illustration of the intense XUV beamline is shown in figure 2.5. The red arrows show the path of the IR radiation while the blue arrows show the path of the XUV radiation.

The XUV beamline at LASC is driven by a chirped pulsed amplification based TeraWatt (TW) laser system. A mode-locked oscillator, of a repetition rate of 80 MHz, with a titanium doped sapphire crystal generates radiation of 800 nm central wavelength. The repetition rate is then reduced to 10 Hz by a pulse picker. As a first step in the CPA process the pulses are being stretched from 100 fs to 300 ps. The stretched pulses are then being amplified to a pulse energy of 400 mJ. These pulses go through a beamsplitter, where one half is send towards the XUV beamline and the other half towards a particle acceleration experiment (not discussed in this thesis) [16, 17].

To generate XUV pulses from the IR pulses, originating from the TW laser system, the IR pulses first need to be recompressed to a pulse duration of about 40 fs with an energy of up to 100 mJ. The pulse energy can be controlled by an attenuator without changing the pulse shape. These pulses are sent in to an evacuated system, with a pressure in the range of 10^{-3} mbar. The pulses are focused, with a focusing mirror, close to a gas nozzle inside the HHG chamber. When the gas nozzle injecting a pulsed gas jet XUV light is generated via HHG.

The generated XUV pulses are sent to the interferometer chamber, where a split and delay unit can split the XUV pulses into two pulses that can be sent in to the experimental chamber with a time delay. This is used for XUV pump-XUV

probe [18]. Right after the interferometer chamber an aluminum filter filters away the remaining IR light.

When the XUV pulses arrive at the experimental chamber they are focused into the center and overlapped with a pulsed gas jet, which arrives from the top of the experimental chamber. The first pulse will start a chemical reaction of the atomic or molecular target while the second one measures the result. With particle spectrometers the generated electrons and ions are recorded simultaneously.

The photodiode in figure 2.5 is a calibrated XUV photodiode and can be used at different locations in the beamline. If it is located directly after the experimental chamber it can be used to measure the photon flux for single XUV shots [19].

Chapter 3

Design and Commissioning

In this work I have designed and integrated an ionization intensity monitor (IIM) in the intense XUV beamline at LASC. In this chapter the design and commissioning of the IIM is described together with the procedures for the data analysis.

3.1 Design

An optimal position to integrate an IIM at the intense XUV beamline in Lund would be directly after the HHG chamber. At this location the IIM can be used as a permanent online photon diagnostic monitor.

In this work a prototype was designed for the purpose of evaluating whether the working principle of an IIM is workable in the XUV beamline. The decision of designing the prototype with parallel plates was made. This makes it suitable to be integrated inside of the HHG chamber, just after the gas nozzle, with the intention to calibrate it against the already existent photodiode, which, at present time, is located just after the experimental chamber.

I decided to design my IIM based on two circular metal plates. The metal plates were separated by porcelain insulators and copper wires were attached to the plates in order to be able to connect the plates to a voltage source. In figure 3.1a the sketch used to manufacture the IIM is shown and in 3.1b the manufactured IIM is shown mounted on a pole inside of the HHG chamber. On the top of the IIM one can observe the copper wires attached to each of the plates.

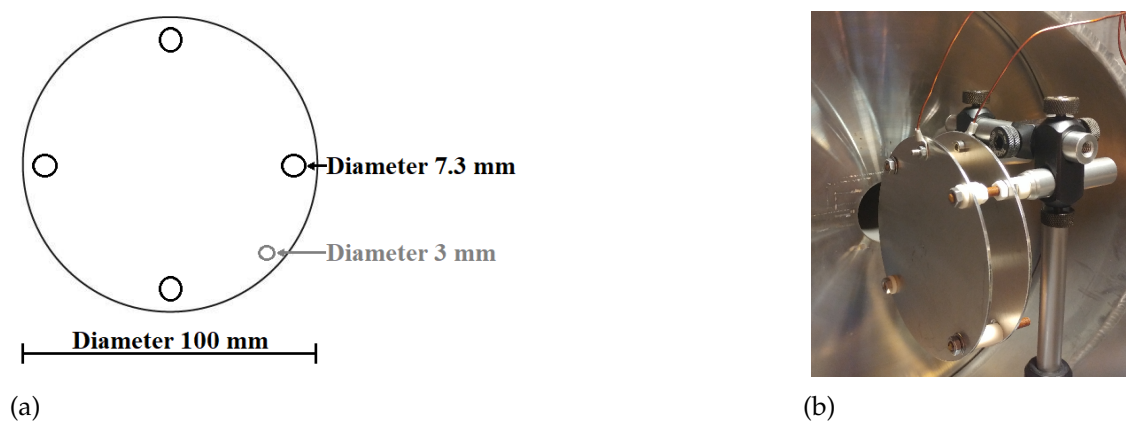(a)   (b)

Figure 3.1: In (a) the sketch used to manufacture the IIM shown in (b).

In figure 3.2a the position of the IIM inside of the HHG chamber is shown. The IIM is placed after the gas nozzle, with respect to the incoming IR pulses, where the XUV pulses are created. The copper wires enters the HHG chamber through a feedthrough and connects one of the plates of the IIM to a voltage supply, while the other one is connected to ground. The copper wires connects the IIM to a voltage supply and an oscilloscope via a decoupling box (DB). Figure 3.2b shows how the voltage source and the oscilloscope are connected to the DB. The red cable to the right of the DB is connected to the IIM inside of the HHG chamber.

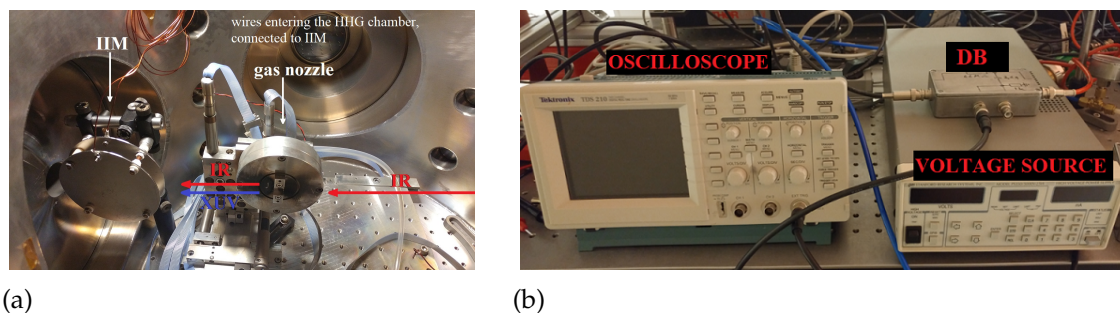(a)   (b)

Figure 3.2: In (a) a picture of the inside of the HHG chamber. The IIM is integrated after the gas nozzle, with respect to the incoming IR pulses, where the XUV pulses are created. In (b) a picture of the the experimental setup is shown, where the voltage source, oscilloscope and DB are marked. The IIM is connected to the DB, not visible in the picture.

3.2   Commissioning

The position of the IIM can only be aligned manually. In order to do that the HHG chamber has to be open, hence it is not possible to generate XUV during the alignment. Instead the IIM was aligned utilizing the incoming IR radiation, by ensuring it passes in between the plates. After the alignment the HHG chamber was closed and a pressure of 10^{-3} mbar was reestablished.

During the generation of high-order harmonics voltage was applied to the IIM and the oscilloscope was used in order to see if there was a signal. At this point a clear signal was obtained at the oscilloscope. To check whether it was XUV or IR that caused the signal the gas jet was delayed, which led to that the signal disappeared and the conclusion that the signal was caused by XUV was made. To scan and save the obtained signals of the photodiode and the IIM the output was put through an ADC card in order to use the software AGAT. In the software the input signal is voltage against time.

Since one of the plates of the IIM is grounded, simultaneous measurements of electrons and ions are not possible. Instead a first measurement with negative voltage applied was performed in order to obtain the signal of the ions. To measure the signal of the ions, single shot measurements of the IIM and the photodiode was performed, during generation of high-order harmonics, simultaneously. While the IR energy was locked to 45 mJ, the applied voltage was varied in steps of 200 V in the range 300-900 V. The measurement for each step in voltage was saved in separate files. For each measurement a reference measurement was

performed, where the gas jet was delayed with 2 ms, in order to determine any change of background-noise due to increased voltage. A known source of noise originates from the Pockel cell in the amplifier in the TW laser system, which switches on and off high voltage for every laser shot and creates electric noise.

The above measurement was reproduced, but with changed polarity, in order to obtain the signal from the electrons. Further, an IR energy scan at three different intensities was performed, while the IIM obtained electrons at an applied voltage of +600 V, to evaluate the linearity between the number of effected electrons and the photon flux.

3.2.1 Data analysis

As mentioned in section 3.2 the single shot measurements were saved in separate files for each different voltage applied. The files contain data of 655 pulses each. To be able to compare the data obtained from the IIM and the photodiode, the files containing the data were analysed using a Matlab script (see appendix A.2).

From each data set the corresponding background data set was subtracted, in order to get rid of noise originating from the Pockel cell.

Due to the linear relation between number of electrons/ions generated and the photon flux (see section 2.2.1 and expression 2.3) we can analyse the area of the peaks. If the signal obtained from the IIM caused by the charge carriers generated by the XUV pulses, the area of the peak, S_{IIM}, should be proportional to the area of the corresponding peak of the photodiode, S_{PD}. In a perfect system they should be directly proportional.

$$S_{IIM} = \int_{a_1'}^{a_2'} F(a')da' \propto S_{PD} = \int_{a_1}^{a_2} G(a)da \qquad (3.1)$$

In expression 3.1 $F(a')$ represents the signal of the IIM, while $G(a)$ represents the signal obtained from the photodiode.

If we assume that $S_{IIM} = k \cdot S_{PD}^n$, where k and n are constants, a linear fit in the logarithmic scale gives the proportionality and due to the logarithm rule

$$log(S_{IIM}) = log(k \cdot S_{PD}^n) = log(k) + log(S_{PD}^n) = log(k) + n \cdot log(S_{PD}) \qquad (3.2)$$

we can obtain n as the slope of the fitted curve.

Chapter 4

Results and Discussion

In this chapter the result of the commissioning of the IIM is presented and discussed. In section 4.1 a summary of the single shot data is shown and explained and in the sections 4.1.1, 4.1.2 and 4.1.3 the data obtained from photodiode, ions and electrons are further described and discussed. Section 4.2 is devoted to the performed IR energy scan.

4.1   Summary of single shot data

In figure 4.1 the mean signal of 655 single shots are shown, together with its respective background noise and the signal when the background is subtracted from the correlated data. Subfigures a, b and c represent the data obtained from the photodiode, d, e and f represents the data obtained from the measurement of ions, with -900 V applied to the IIM. Subfigures g, h and i represent the data obtained from the measurement of electrons, with +900 V applied to the IIM. Notice that the vertical axis (amplitude) on the panels representing the ions differ from the vertical axis in panels representing the photodiode and the electrons.

In the sections 4.1.1, 4.1.2 and 4.1.3 the data obtained from photodiode, ions and electrons are further described and discussed.

(a) Photodiode signal   (b) Photodiode background   (c) Photodiode signal corrected

(d) Ion signal   (e) Ion background   (f) Ion signal corrected

(g) Electron signal   (h) Electron background   (i) Electron signal corrected
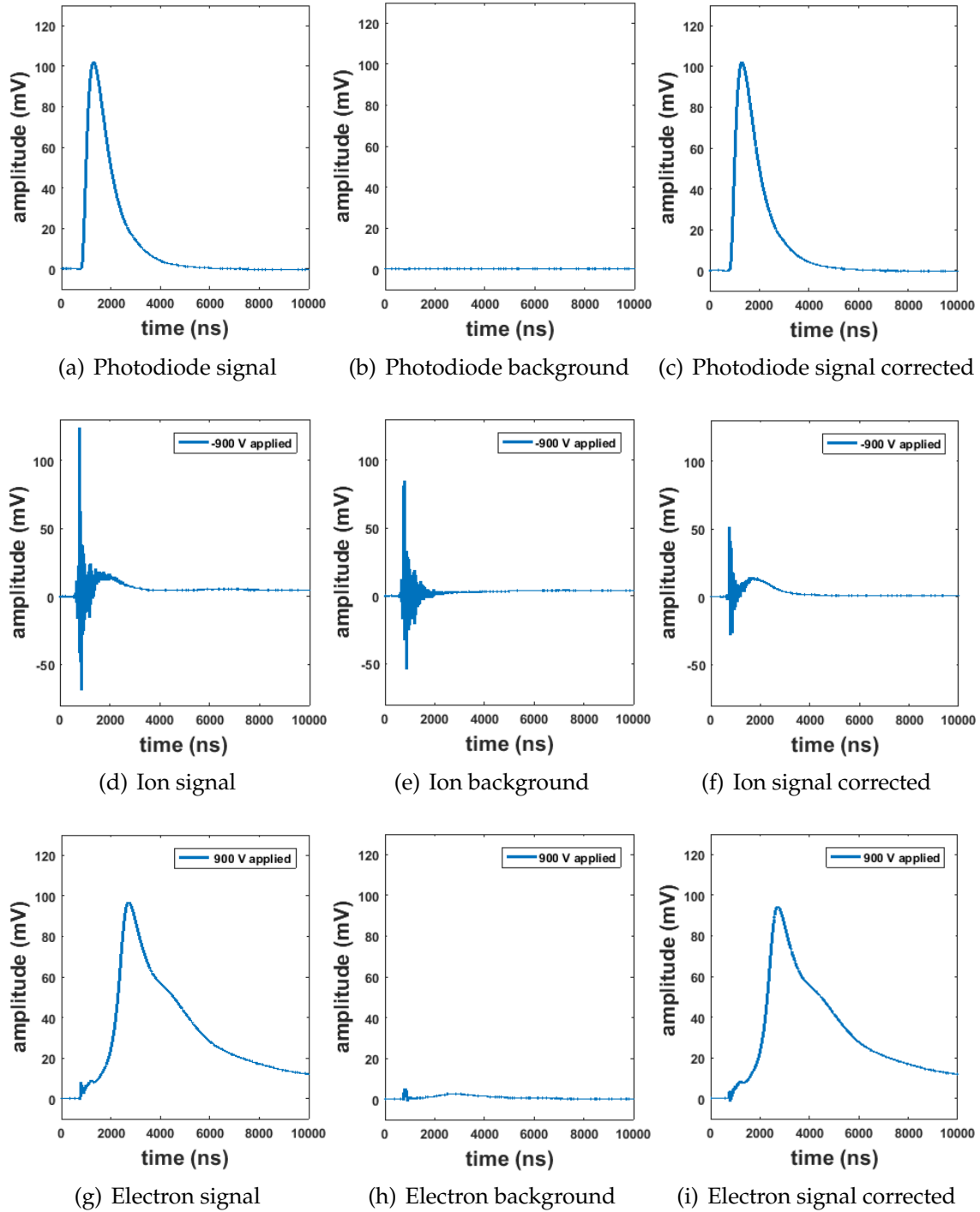
Figure 4.1: A summary of the obtained signal. In figure a,b and c the signal, background and signal corrected for background of the photodiode are shown. Figure d,e and f represent the obtained signal when ions were measured with the IIM and figure g,h and i represent the obtained signal when electrons were measured with the IIM. Notice the different scale of the amplitude for the ions plot compared to photodiode and electrons.

4.1.1 Photodiode

In figure 4.1 a, b and c the calibrated XUV photodiode is shown. This is the data used to compare the obtained signals for ions and electrons. The background clearly shows that there is no XUV pulse when the jet is delayed.

4.1.2 Ions

As can be observed in figure 4.1 d, e and f, there is a lot of background noise, mainly due to the electric noise originating from the Pockel cell of the laser. We have not been able to explain why there is more noise when negative voltage is applied compared to positive voltage applied (compare figure d, e, f with figure g, h, i). The Pockel cell noise can be used as an indication of when the pulses arrive, hence where time zero is. In figure 4.1f the Pockel cell noise is obtained at ~ 770 ns, hence our time zero is ~ 770 ns. From equation 2.6, the travel time of the ions at -900 V applied is ~ 430 ns and by adding the experimental time zero the ions should appear at 1200 ns. In figure 4.1c one can observe that there is a signal in the time range of 1000-3000 ns, just about after the Pockel cell noise.

In figure 4.2 zoom-ins of the mean signals, at the time range 900-3000 ns, for different applied voltage are shown. Even though the background noise is subtracted from the signal there is still a lot of Pockel cell noise left. We can also see oscillations in the measurements of different voltage applied with a frequency of ~ 16 MHz, except for the -900 V measurement, where the frequency of the oscillation is ~ 35 MHz. These oscillations are likely caused by the electronic devices.

The expected behaviour of the signals, due to increasing voltage, is larger peak area and a shorter arrival time, discussed in section 2.2.3. We can see in figure 4.2 that the peak area increases with increasing voltage. However, due to a large amount of noise it is not possible to obtain whether the arrival time decreases with increasing voltage. We can only say that the ions arrive after 770 ns, which is the experimental time zero.
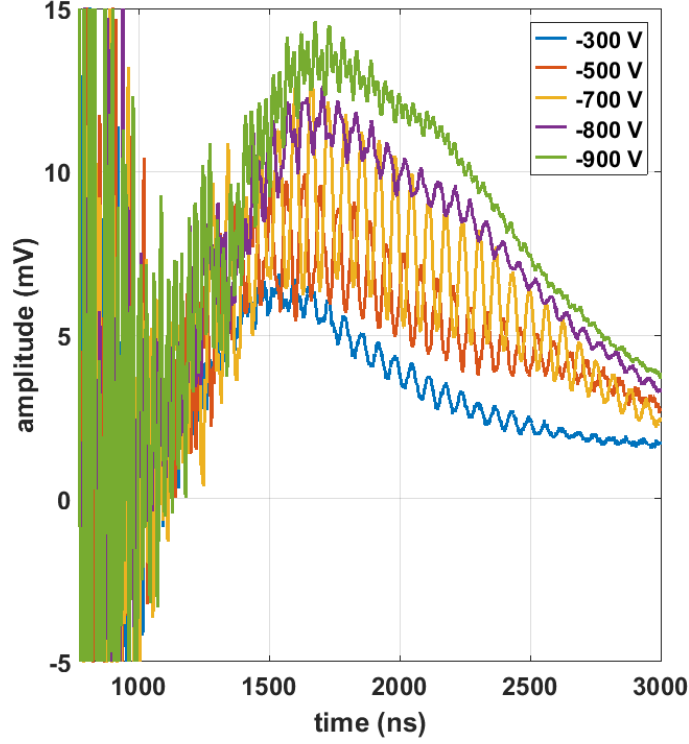
Figure 4.2: Zoom of the mean signals from each measurement for ions with different voltage applied to the IIM, over the time range 770-3000 ns.

4.1.3 Electrons

Due to that the ions signal was strongly contaminated by Pockel cell noise a decision to analyse the electron signal in more depth was made. In figure 4.1 g, h and i, we can observe a large peak around 3000 ns. However, since we know that the ions arrive around 1200 ns and the fact that the experimental time zero is 770 ns, this can not be the signal from the electrons generated by the XUV radiation. The large peak might be coming from the plasma that is generated inside of the HHG chamber during generation of high-order harmonics, where plasma is a gas of charged particles unbounded to each other which is overall neutrally charged. However, due to the charged particles it is electrically conductive.

In figure 4.1i one can obtain two signals arriving before the large peak. By calculations of the travel time for the electrons we can obtain where in the spectrum the signal of the electrons should appear. By using the expression 2.6 the arrival time for the electron signal, with +900 V applied to the IIM, can be calculated to

$$t = d\sqrt{\frac{m_e}{q(V_A - V_C)}} = 20 \cdot 10^{-3}\sqrt{\frac{9.11 \cdot 10^{-31}}{1.602 \cdot 10^{-19} \cdot 900}}\, \text{s} \approx 1.6\, \text{ns}.$$

The arrival time of the electrons is hence about 2 ns second from time zero, which indicates that the most left peak in the spectrum is the electron peak. In figure 4.3 zoom-ins of the mean signals, in the time range 760-790 ns, for different applied voltages is shown. As mentioned in the previous section, there is much less noise from the measurement with positive voltage applied, which can be observed in the figure. Hence one can clearly see the decreasing arrival time

17

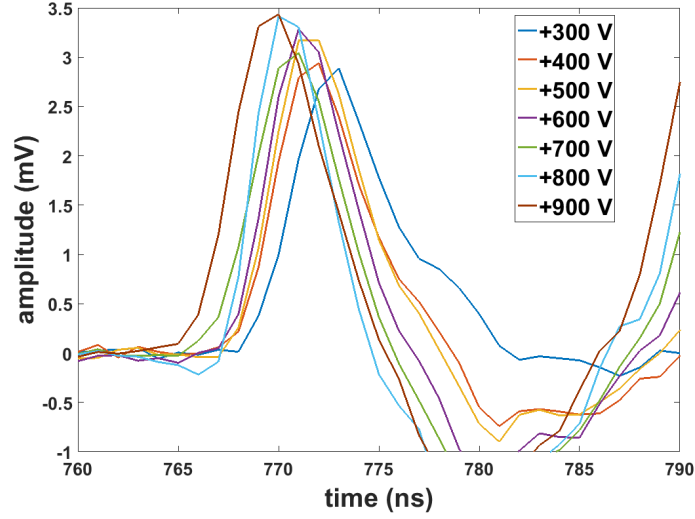corresponding to the increasing voltage as well as the increasing peak area due to increasing voltage.

Figure 4.3: Zoom of the mean signals from each measurement for electrons with different voltage applied to the IIM, over the time range 760-790 ns.

The ions generated, during measurement of electrons, are accelerated towards the grounded plate in the IIM. When ions hit the plate they can either absorb or kick out electrons from the plate. Kicked out electrons create a current of secondary electrons accelerating towards the detector plate. This secondary electrons will generate a signal in our measurement. As for primary electrons we look at the electron signal with +900 V applied to the IIM. To calculate the travel time of the secondary electrons, the travel time for the ions hitting the grounded plate is added with the travel time for secondary electrons hitting the detector plate. This is calculated to be

$$
t = d\sqrt{\frac{m_{ion}}{q(V_A - V_C)}} + d\sqrt{\frac{2m_e}{q(V_A - V_C)}}
$$

$$
= 20 \cdot 10^{-3} \left(\sqrt{\frac{40 \cdot 1.66 \cdot 10^{-27} - 9.11 \cdot 10^{-31}}{1.602 \cdot 10^{-19} \cdot 900}} + \sqrt{\frac{2 \cdot 9.11 \cdot 10^{-31}}{1.602 \cdot 10^{-19} \cdot 900}} \right) \text{s}
$$

$$
\approx 430\,\text{ns}.
$$

This gives an arrival time of about 1200 ns, when account for time zero as 770 ns, for the secondary electrons. In figure 4.4 zoom-in of the mean signals, at the time range 750-1500 ns, for different applied voltage are shown. The calculated arrival time indicates that the smooth peak in the time range 900-1400 ns is the signal of the generated secondary electrons.
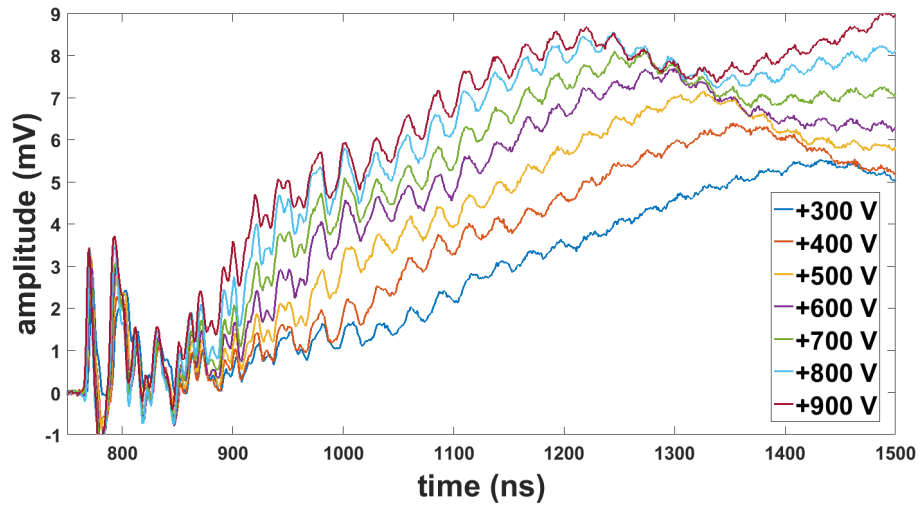
18

Figure 4.4: Zoom of the mean signals from each measurement for electrons with different voltage applied to the IIM, over the time range 750-1500 ns.

4.2 Linearity

An IR energy scan was made for the purpose of evaluating the linearity between generated charge carriers and the intensity of the radiation (See section 2.2.1 and expression 2.3)). As stated in the previous section, the ion signal contains to much noise for further investigation. For the electron signal both the primary and secondary peak areas are much smaller compared to the area peak of the photodiode measurement, hence the decision of using the whole spectrum for the IR energy scan was made. Even though it contains the large peak which might be coming from the plasma it might indicate the linearity.

The IR energy scan was performed at the energies 30,40 and 48 mJ, while electrons were measured by the IIM, with an applied voltage of +600 V. In figure 4.5 the obtained evaluation of the linearity is shown.

The slope of the fitted curve tells us that the linear relation between number of electrons and photon flux is about 0.7. Possible cause of the deviation from 1 is the low statistic in the measurement and the fact that the plasma signal might not be directly proportional to the XUV pulse energy.
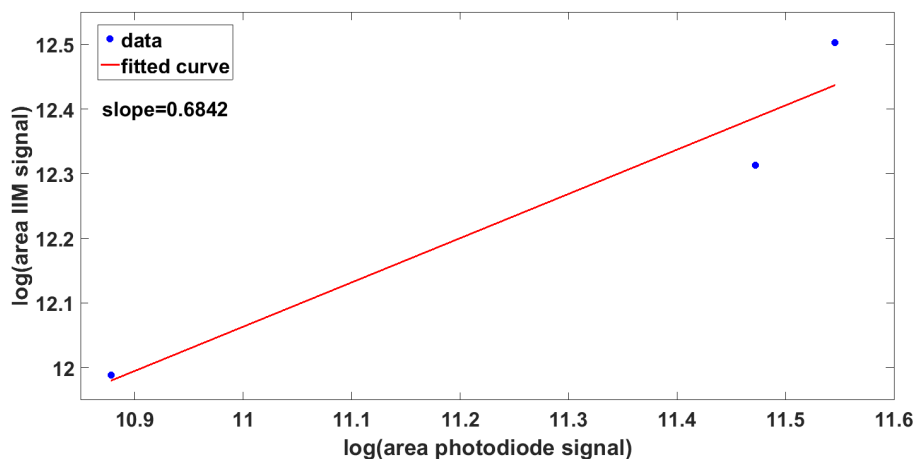

Figure 4.5: Evaluation of the IR energy scan in log-log scale. Performed at energies 30,40 and 48 mJ, while IIM measured electrons at an applied voltage of +600 V.

Chapter 5

Summary and Outlook

With inspiration from GMDs currently used at FLASH, I have designed an IIM with parallel plates and integrated it in the intense XUV beamline at LASC. The working principle of the IIM is based on photoionization of rare gases with intense, pulsed XUV radiation.

During commissioning of the IIM it was shown that the IIM is not sensitive to IR, however sufficiently sensitive to XUV pulses to obtain both ion and electron signal. Single shot measurements determine the correlation between travel time of charge carriers and induced potential. The IR energy scan indicates the linearity between the number of generated electrons, during generation of high-order harmonics, and photon flux.

To further investigate the practical working principle of the IIM in the XUV beamline, the design, and further on its location, need to be developed. By developing the current design such that one can apply voltage to both of the plates would make it possible to measure ions and electrons simultaneously. This would make the data obtained from ions and electrons not only comparable to the data obtained from the photodiode but also comparable with respect to each other. Further on, it might suppress the signal caused by assumed plasma signal, due to an extension in the electric field that will hinder the charge carriers from the plasma source to contaminate the measurement.

In the future the aspiration is to develop an IIM that can be integrated in the intense XUV beamline after the HHG chamber. At this location the pressure can be stabilized and the measurement would not be contaminated by charge carriers from the plasma source.

Acknowledgements

Bibliography

[1] Tiedtke K, Feldhaus J, Hahn U, Jastrow U, Nunez T, Tschentscher T, et al. *Gas detectors for x-ray lasers.* Journal of applied physics. 2008;**103**(9):094511(1-7)

[2] Mainman T.H. *Stimulated optical radiation in ruby.* Nature. 1960;**187**(4736):493-4

[3] Westfälische Wilhelms-Universität Münster. *The free electron laser FLASH* [Internet].[cited 2019-06-13] Available from: `https://www.uni-muenster.de/Physik.PI/Zacharias/en/research/fel/free_electron_lasers.html`

[4] Westfälische Wilhelms-Universität Münster. *High-order harmonic generation* [Internet]. [cited 2019-06-13] Available from: `https://www.uni-muenster.de/Physik.PI/Zacharias/en/research/hh/hhg.html`

[5] Murphy J.B and Pellegrini C. *Free electron lasers for the XUV spectral region.* Nuclear instruments and methods in physics research. 1985;**237**(1-2):159-67

[6] Ferray M, L'Huillier A, Li X.F, Lompre L.A, Mainfray G and Manus C. *Multiple-harmonic conversion of 1064 nm radiation in rare gases.* Journal of physics B:atomic,molecular andd optical physics.1988;**21**(3):L31–5

[7] Sorokin A.A, Gottwald A, Hoehl A, Kroth U, Schöppe H, Ulm G, et al. *Method based on atomic photoionization for spot-size measurement on focused soft x-ray free-electron laser beams.* Applied physics letters. 2006;**89**(22):221114(1-3)

[8] Manschwetus B, Rading L, Campi F, Maclot S, Coudert-Alteirac H, Lahl J et al. *Two-photon double ionization of neon using an intense attosecond pulse train.* Physical review A. 2016;**93**(6):061402(1-5)

[9] Ritcher M, Gottwald A, Kroth U, Sorokin A.A, Bobashev S.V, Schmaenok L.A, et al. *Measurement of gigawatt radiation pulses from a vacuum and extreme ultraviolet free-electron laser.* Applied physics letters. 2003;**83**(14):2970-2

[10] Eichholz G.G, Poston J.W. *Principles of nuclear radiation detection.* 1. ed. Atlanta,Georgia: Ann Arbor Science;1979. pp. 42,89-110.

[11] Lovelock J.E. *Ionization methods for the analysis of gases and vapors.* Analytical chemistry, American chemical society. 1961;**33**(2):162-78

[12] Samson J.A.R, Stolte W.C. *Precision measurement of the total photoionization cross-sections of He,Ne,Ar,Kr and Xe.* Journal of Electron Spectroscopy and Related Phenomena. 2002;**123**(2-3):265–76

[13] Sorokin A. A, Wellhöfer M, Bobashev S.V, Tiedtke K, and Richter M. *X-ray-laser interaction with matter and the role of multiphoton ionization: Free-electron-laser studies on neon and helium.* Physical Review A. 2007;**75**(5):051402(1-4)

[14] Young H.D, Freedman R.A. *Sears and Zemansky's University physics with modern physics.* Scandinavian 14. ed. Edingburgh,England:Pearson education limited;2016. p 777

[15] Sharpe J. *Nuclear radiation detectors.* 2. ed. London:Methuen CO.LTD; 1964. pp. 154-9

[16] Svanberg S, Larsson J, Persson A and Wahlström C-G. *Lund high-power laser facility -systems and first results.* Physica scripta. 1994;**49**(2):187-97

[17] Lahl J. *Investigation of ultrafast molecular dynamics via covariance mapping: A tool for intense XUV light sources.* Sweden: Lund University;2019. pp. 22-5

[18] Wikmark H. *Spatial and temporal aspects of intense attosecond pulses for pump-probe experiments.* Sweden: Lund University;2019. pp 21-30

[19] Rading L. *An intense attosecond light source-from generation to application.* Sweden: Lund University;2017. pp 46-50

Appendix A

Appendices

A.1 Design of IIM

The material used for the design was stainless steel 316. In the table below the dimensions of the manufactured IIM are stated.

Diameter of plate	100 mm
Thickness of plate	1 mm
Length of porcelain insulator	20 mm
Diameter of hole to attach insulators	7.5 mm
Diameter of hole to attach copper wire	3 mm

A.2 IR energy scan

The code presented in this section was used to evaluate the linearity of the generated electrons and the photon flux.

```
clear all;
close all;

addpath('\\fysfile01\atomhome$\ha2204be\My Documents\MATLAB\From Jasper\AGATAnalyse')
path='\\fysfile01\atomhome$\ha2204be\My Documents\MATLAB\2019-04-02\';
file={'GMD_PD_25deg__0000.lma';'GMD_PD__0000.lma';'GMD_PD_35deg__0000.lma';
'GMD_PD_25deg__0000.lma';'GMD_PD__0000.lma';'GMD_PD_35deg__0000.lma'};

for j=1:length(file)
    [data, header, ~] = ReadAGATdata(path,char(file(j)));
 if j<4

  channel_used=1;
  NoiseLevel=header.channels(channel_used).Noise;
  CountingMode=NoiseLevel>0;

  [TOFSpectrum(:,:,j),TOFAxes] = ExtractTOF(data,header,channel_used,CountingMode);
  for i=1:size(TOFSpectrum,2)
    TOFSpectrum(:,i,j)=-TOFSpectrum(:,i,j)
    % flip around zero
    TOFSpectrum(:,i,j)=TOFSpectrum(:,i,j)-mean(TOFSpectrum(14000:20000,i,j));
    % set the baseline to zero

    if sum(TOFSpectrum(700:5000,i,j))>0
        TOFSpectrum_sum(i,j)=sum(TOFSpectrum(700:5000,i,j));
        % sum of raw data
      end
```

```
      end
      mean_TOF(:,j) = mean(TOFSpectrum(:,:,j)');
      % mean for each set of shots in the files

        if sum(mean_TOF(700:5000,j))>0
         mean_TOF_sum(j) = sum(mean_TOF(700:5000,j));
          % sum of mean curves
        end
  end


  if j >= 4
   channel_used=2;
   NoiseLevel=header.channels(channel_used).Noise;
   CountingMode=NoiseLevel>0;

   [GMDSpectrum(:,:,j-length(file)/2),GMDAxes] = ExtractTOF(data,header,channel_used,CountingMode);

   for k=1:size(TOFSpectrum,2)
      GMDSpectrum(:,k,j-length(file)/2)=GMDSpectrum(:,k,j-length(file)/2);
      % flip around zero
      GMDSpectrum(:,k,j-length(file)/2)=GMDSpectrum(:,k,j-length(file)/2)-mean(GMDSpectrum(1:600,k,j-length(file)/2));
      % set the baseline to zero

        if sum(GMDSpectrum(1500:10000,k,j-length(file)/2))>0
         GMDSpectrum_sum(k,j-length(file)/2)=sum(GMDSpectrum(1500:10000,k,j-length(file)/2));
          % sum of raw data
        end
   end
   mean_GMD(:,j-length(file)/2) = mean(GMDSpectrum(:,:,j-length(file)/2)');
   % mean for each set of shots in the files

        if sum(mean_GMD(1500:10000,j-length(file)/2))>0
          mean_GMD_sum(j-length(file)/2) = sum(mean_GMD(1500:10000,j-length(file)/2));
        end
   end
end


fit_GMD_TOF_mean = fit(log(mean_TOF_sum'),log(mean_GMD_sum'),'poly1');
figure
plot(fit_GMD_TOF_mean,log(mean_TOF_sum'),log(mean_GMD_sum'));
```

A.3   Single shot measurement

The code presented in this section was used to analyse the single shot measurements for ions and electrons, where different voltage was applied to the IIM.

```
clear all;
close all;

addpath('\\fysfile01\atomhome$\ha2204be\My Documents\MATLAB\From Jasper\AGATAnalyse')
path='\\fysfile01\atomhome$\ha2204be\My Documents\MATLAB\positivepolarity\';
path='\\fysfile01\atomhome$\ha2204be\My Documents\MATLAB\positivepolarity\';

file1={'NEW300V_jeton__0000.lma';'NEW400V_jeton__0000.lma';'NEW500V_jeton__0000.lma';'NEW600V_jeton__0000.lma';
    'NEW700V_jeton__0000.lma';'NEW800V_jeton__0000.lma';'NEW900V_jeton__0000.lma';
    'NEW300V_jeton__0000.lma';'NEW400V_jeton__0000.lma';'NEW500V_jeton__0000.lma';'NEW600V_jeton__0000.lma';
    'NEW700V_jeton__0000.lma';'NEW800V_jeton__0000.lma'};
file2={'NEW300V_jetoff__0000.lma';'NEW400V_jetoff__0000.lma';'NEW500V_jetoff__0000.lma';'NEW600V_jetoff__0000.lma';
    'NEW700V_jetoff__0000.lma';'NEW800V_jetoff__0000.lma';'NEW900V_jetoff__0000.lma';'NEW300V_jetoff__0000.lma';
    'NEW400V_jetoff__0000.lma';'NEW500V_jetoff__0000.lma';'NEW600V_jetoff__0000.lma';'NEW700V_jetoff__0000.lma';
    'NEW800V_jetoff__0000.lma';'NEW900V_jetoff__0000.lma'};

areapoint1 = [3500,2800,1800,1500,1500,1100,1300];          % area points for GMD peaks
areapoint2 = [18100,12000,12000,12000,10000,10000,10000];
```

```
for j=1:length(file1)
 [data, header, ~] = ReadAGATdata(path,char(file1(j)));
 if j<8
  channel_used=1;
  NoiseLevel=header.channels(channel_used).Noise;
  CountingMode=NoiseLevel>0;
  [TOFSpectrum(:,:,j),TOFAxes] = ExtractTOF(data,header,channel_used,CountingMode);

   for i=1:size(TOFSpectrum,2)
     TOFSpectrum(:,i,j)=-TOFSpectrum(:,i,j);                               % flip around zero
     TOFSpectrum(:,i,j)=TOFSpectrum(:,i,j)-mean(TOFSpectrum(1:600,i,j));   % set the baseline to zero

        if sum(TOFSpectrum(750:6000,i,j))>2500
         TOFSpectrum_sum(i,j)=sum(TOFSpectrum(750:6000,i,j));
        end
    end
 end

 if j>=8
  channel_used=2;
  NoiseLevel=header.channels(channel_used).Noise;
  CountingMode=NoiseLevel>0;
  [GMDSpectrum(:,:,j-length(file1)/2),GMDAxes] = ExtractTOF(data,header,channel_used,CountingMode);

    for k=1:size(GMDSpectrum,2)  % flip around zero

     if sum(GMDSpectrum(areapoint1(j-length(file1)/2):areapoint2(j-length(file1)/2),k,j-length(file1)/2))>200;
                GMDSpectrum_sum(k,j-length(file1)/2)=
                sum(GMDSpectrum(areapoint1(j-length(file1)/2):areapoint2(j-length(file1)/2),k,j-length(file1)/2));
                 % give a 655x7 matrix with each element an areavalue /655spectrum/file
      end
    end
 end
end


%% Background noise
for j=1:length(file2)
    [data, header, ~] = ReadAGATdata(path,char(file2(j)));

    if j<8
     channel_used=1;
     NoiseLevel=header.channels(channel_used).Noise;
     CountingMode=NoiseLevel>0;
     [TOFSpectrum_jettoff(:,:,j),TOFAxes] = ExtractTOF(data,header,channel_used,CountingMode);

  for i=1:size(TOFSpectrum_jettoff,2)
    TOFSpectrum_jettoff(:,i,j)=TOFSpectrum_jettoff(:,i,j)-mean(TOFSpectrum_jettoff(1:600,i,j));
    % set the baseline to zero
    TOFSpectrum_sum_jettoff(i,j)=sum(TOFSpectrum_jettoff(:,i,j));

  end
 end
    if j>=8
     channel_used=2;
     NoiseLevel=header.channels(channel_used).Noise;
     CountingMode=NoiseLevel>0;
     [GMDSpectrum_jettoff(:,:,j-length(file2)/2),GMDAxes] = ExtractTOF(data,header,channel_used,CountingMode);

     for k=1:size(GMDSpectrum_jettoff,2)
     GMDSpectrum_jettoff(:,k,j-length(file2)/2)-mean(GMDSpectrum_jettoff(1:600,k,j-length(file2)/2));
     % set the baseline to zero
       GMDSpectrum_sum_jettoff(i,j-length(file2)/2)=sum(GMDSpectrum_jettoff(:,k,j-length(file2)/2));
        % give a 655xfiles matrix with each element an areavalue /655spectrum/file
      end
 end
end


%% mean curves GMD

%jet on
for j=1:length(file1)/2
```

```matlab
    GMDSpectrum_jo(:,:,j) = GMDSpectrum(:,:,j)';
    mean_GMD_jeton(:,j) = mean(GMDSpectrum_jo(:,:,j));
  end


%background noise
for j=1:length(file2)/2
    GMDSpectrum_jf(:,:,j) = GMDSpectrum_jettoff(:,:,j)';
    mean_GMD_jettoff(:,j) = mean(GMDSpectrum_jf(:,:,j));
  end


% background noise subtracted from jet on
for j=1:length(file1)/2
    difference(:,:,j)=GMDSpectrum(:,:,j)-GMDSpectrum_jettoff(:,:,j);
    mean_difference(:,j) = mean(difference(:,:,j)');
end


%%  mean-curve PD
% jet on

for j=1:length(file1)/2
    TOFSpectrum_jo(:,:,j) = TOFSpectrum(:,:,j)';
    mean_TOF_jetton(:,j) = mean(TOFSpectrum_jo(:,:,j));
  end


% background noise

for j=1:length(file2)/2
    TOFSpectrum_jf(:,:,j) = TOFSpectrum_jettoff(:,:,j)';
    mean_TOF_jettoff(:,j) = mean(TOFSpectrum_jf(:,:,j));
  end


% background noise subtracted from jet on

for j=1:length(file2)/2
    mean_curves_PD(:,j) = mean_TOF_jetton(:,j)-mean_TOF_jettoff(:,j);        % mean for each file
end
```